scientific reports

Check for updates

OPEN

Beyond growth: comparative impact of plastics and natural particles on EPS dynamics and aggregation in *Rhodomonas Salina*

Marie Sioen[1,2,3]✉, Peter Chaerle[2], Maaike Vercauteren[1], Ronny Blust[3], Raewyn M. Town[3], Colin Janssen[1] & Jana Asselman[1]

Understanding the ecological impact of micro- and nanoplastics (MNPs) requires going beyond traditional growth inhibition endpoints. The authors have investigated the comparative effects of plastics, namely virgin polyethylene terephthalate (vPET), weathered PET (wPET), and the natural particle kaolin on the algae-bacteria consortium of the microalga *Rhodomonas salina*, with analysis of growth dynamics, extracellular polymeric substance (EPS) production, and aggregation behaviour in terms of number, size and composition. Maximum growth inhibition values between 53.32% and 67.05% were observed. Both wPET and kaolin caused stronger and earlier growth inhibition than vPET, and their effects were significantly correlated with increased EPS production indicating a coordinated stress response. The protein fraction of the bound EPS was affected the most, with observed increases between 165.6% and 422.2%. Furthermore, particle exposure increased the number, size and composition of aggregates formed, while highlighting the role of bacteria in microbial aggregation processes. The similar biological responses induce by wPET and kaolin suggest that particle properties, rather than material identity, predominantly drive algal stress and aggregation patterns. The observed responses reflect not merely individual algal stress, but highlight the emergent properties of the microbial consortium, with EPS acting as a central mediator with ecosystem-scale implications. This study takes a first step in exploring the impact of ecologically relevant MNPs on an algae–bacteria consortium, addressing a well-recognized gap in the existing literature.

Keywords Micro-algae, EPS, Aggregation, Weathered control, Natural particle control

Abbreviations

μmax	Maximum growth rate
ATR-FTIR	Attenuated Total Reflection - Fourier Transformed Infrared spectroscopy
B-EPS	Bound-EPS
CCAP	Culture Collection of Algae and Protozoa
Dav	Average diameter
D10	10% of particles has a diameter smaller than this value
D90	90% of particles has a diameter smaller than this value
DI	Deionized Water
DLS	Dynamic Light Scattering
DPPC	Dipalmitoylphosphatidylcholine
EM	Electrophoretic Mobility
EPS	Extracellular Polymeric Substances
EPSc	Carbohydrate fraction EPS
EPSp	Protein fraction EPS
FCM	Flow Cytometry
HD	Hydrodynamic diameter

[1]Blue Growth Research Lab, Ghent University, Ostend Science Park, Wetenschapspark 1, Ostend 8400, Belgium. [2]Department of Biology, Protistology and Aquatic Ecology, Ghent University, Krijgslaan 281 – S8, Ghent 9000, Belgium. [3]ECOSPHERE, Department of Biology, University of Antwerp, Groenenborgerlaan 171, Antwerpen 2020, Belgium. ✉email: marie.sioen@ugent.be

ICP-MS	Inductively coupled plasma - Mass Spectrometry
iFCM	Imaging Flow Cytometry
IQR	Interquartile Range
JRC	Joint Research Centre
K	Carrying capacity
MNP	Micro- and Nanoplastics
OLS	Ordinary Least Squares
P/C ratio	Protein/Carbohydrate ratio
PS	Polystyrene
RRS	Residual Sum of Squares
Std Dev	Standard Deviation
SD	Size Distribution
SEM	Scanning Electron Microscope
S-EPS	Soluble-EPS
vPET	Virgin PET
wPET	Weathered PET
ZP	Zeta Potential

Micro-algae, the algae-bacteria consortium and EPS

Micro-algae are crucial in maintaining healthy aquatic ecosystems and regulating the global carbon cycle. Yearly, 45 billion tons of new phytoplankton are produced, making them responsible for 50% of the total primary production[1]. Micro-algae form the basis of aquatic food webs. Their production rate determines the energy flow to all higher trophic levels[2,3] while the sinking of dead micro-algae contributes the storage of carbon in the deep ocean, known as the *biological carbon pump*[4].

In aquatic environments, algae coexist with bacteria, in what is often referred to as the *algae-bacteria continuum*, with interactions ranging from mutualism to parasitism, influencing nutrient cycling, organic matter processing, and overall ecosystem stability[5]. For example, it is reported that Extracellular Polymeric Substances (EPS) produced by algae provide a nutrient rich and protective environment, thus attracting heterotrophic bacteria[6]. Bacteria, in turn, were shown to promote the aggregation of algae and bacteria, by attaching to algae cell-surfaces, thereby stimulating the production of EPS[7]. The interactions between algae and bacteria in a consortium can give rise to properties that do not emerge from either partner alone. These are system-level responses, often referred to as *emergent properties*[8]. Therefore, as EPS production is a property of the consortium (both algae and bacteria use and produce EPS), rather than of the individual species, tracing the origin of EPS production in algae-bacteria interactions is challenging[6].

The composition and structure of EPS produced by aquatic micro-organisms depend on the species involved, and growth conditions, with proteins and polysaccharides as the primary components[9,10]. Several EPS functionalities have been identified and categorized, including constructive, adsorptive, active- and surface active, informative and nutritive functions[11,12]. EPS can remain closely attached to the cell (bound EPS; B-EPS) or disperse freely in the water (soluble EPS; S-EPS)[13,14]. Increased EPS production and aggregation is a widely acknowledged protection mechanism of microbial consortia[15]. For example, Chen et al., (2015) observed increased EPS production by *Chlorella vulgarus* after exposure to cadmium, while Mona and Kaushik (2015) observed similar increases by *Nostoc linckia* after exposure to chromium and cobalt[16,17]. Micro- and nanoplastics (MNPs) also cause increased EPS production as a stress response, as has recently been demonstrated by Li et al., (2023) for PS (0.1 and 1 µm, 1.91×10^6 – 1.91×10^{11} Particles ml^{-1} (Ps ml^{-1}), *Scenedesmus quadricuada*), as well as by Khatiwada et al., (2023) for PET (300 µm, 25–200 mg L^{-1}, *Scenedesmus sp.*), and by Su et al., (2022) for PE, PA, PLA and PBS (53–76 µm, 100–1000 mg L^{-1}, *Chlorella vulgaris*)[18–20].

Additionally, EPS is a known bio-flocculant. Its sticky nature - due to functional groups including carboxyl, hydroxyl and amino groups making EPS predominantly negatively charged - promotes aggregation of algae, bacteria, and biotic and abiotic debris[12,21]. This property has been investigated for biotechnological applications[9,21–23] but can also have far-reaching ecological consequences. Marine snow, the organic fraction of the carbon pump, consists mainly of EPS mediated aggregates and feacal pellets[12]. Changes in the quantity, size, and density of aggregates can significantly impact carbon transport to the ocean floor[24,25]. Furthermore, changes in food size (changed aggregate size distribution), and changes in food availability (aggregation affects sinking rate), may disrupt the marine food web[26,27].

While the effects of MNPs on algae growth and algae EPS production is well-documented, information on their effect on the interactions within an algae-bacteria consortium remain scarce[28]. However, You et al., concluded in 2021 that algae-bacteria interactions are sensitive to pollutants[29]. For example, Huang et al., (2022) observed how PS MPs could damage the structural stability of algae-bacterial granular sludge (ABGS)[30] and Hao et al., (2023) observed that NPs significantly affect bacteria community structure, but leave algae community unaffected in aquatic ecosystems dominated by submerged macrophytes[31].

This work builds further upon previous work by the same authors, demonstrating that MNPs cause coupled algae growth inhibition and increased EPS production[32]. In the presented study, the effects of three types of micro- and nano particles (MNPs),virgin PET (vPET, D_{av} = 710 nm), weathered PET (wPET, D_{av} = 740 nm), and the natural mineral kaolin (D_{av} = 830 nm) ,were investigated on the consortium of the marine microalga *Rhodomonas salina* and its associated bacteria. When the authors refer to "algae" in the paper, they talk about the entirety of the algae cells and its associated bacteria. By comparing natural versus synthetic, and virgin versus weathered particles, this experimental design allowed for the disentanglement of the contribution of particle properties to biological responses and stress mechanisms in algae. The polymer PET was chosen as the focus of this study because, despite being the third most produced type of plastic waste[33] its effects on the

marine environment remain largely understudied, with only 3 papers available on effects of PET on marine microalgae[32,34,35]. Algae were exposed for twelve days to four concentrations (10, 100, 1000, and 10000 particles ml^{-1}), with measurements taken at multiple time points along their growth curve. The impact on both algae-specific endpoints, such as algae growth dynamics, as well as emergent endpoints of the consortium, such as the production and composition of both bound and soluble EPS, as well as on aggregate formation and the algae-bacteria interactions within the aggregates was evaluated. This study initiates an exploration into the effects of ecologically relevant MNPs on algae–bacteria consortia, tackling a critical knowledge gap in current research.

Results

Relevance and research gap

To the best of our knowledge, 93 research articles (as of March 2025) discussing MNP on microalgae, covering 119 distinct experimental designs are published (see SI. 1 for details). However, significant gaps remain. Despite PET being the third most common polymer type in plastic waste in 2019 (7.02%, following PE and PP), only nine publications investigated its effects on microalgae, with only three reports studying marine microalgae[33]. Furthermore, while environmental plastic particle concentrations increase with decreasing particle size, only 42 experiments included plastics smaller than 1 µm[36] and only one of these used concentrations below 10×10^4 Ps ml^{-1}, a level considered environmentally relevant. Environmental monitoring typically does not consider plastic particles smaller than 1 µm. Thus, to obtain a rough estimate of the potential concentrations of small particles, simple mass conversion can be employed[37]. For example, a measured environmental plastic concentration of 0.058 Ps m^{-3} with a mean size (length of largest dimension) of 2.75 mm[38] would translate to a MP concentration of 1.21×10^3 Ps ml^{-1} of particles with a diameter of 1 µm. Furthermore, seventeen literature reports included aged or weathered particles, but only one studied PET. Weathered particles have gone through physical and chemical changes[39] which causes altered particle behaviour and stability in aqueous media, modified interaction with aquatic organisms and potentially changed toxicity[40–43]. Including weathered MNPs in toxicity assessments reflects more accurately ecologically relevant conditions[44] and reduces the need for surfactants[40,45]. Only three experiments included a natural particle control, two with PET. In natural environments, algae are continuously exposed to natural particles[46]. Including a natural particle control allows for the disentanglement of plastic-specific effects from general particle effects, and the assessment of the ecological relevance of plastic toxicity[43]. Positioning our study within the MNP toxicity research field, it becomes evident that our experimental design was not only highly relevant due to its environmental realism but also unique. To date, no other study has combined PET as a test polymer with both a weathered particle control and a natural particle control, while also focusing on particles smaller than 10 µm in diameter at concentrations below 10×10^4 Ps ml^{-1}.

Growth dynamics

R. salina cell density was measured on multiple timepoints (Fig. 1) using flow cytometry over the course of 12 days. The algae followed a typical microalgal growth curve as described in literature[47] starting with a lag phase (until day 2), followed by the exponential growth phase (until day 7), and the stationary phase (SI. 8). All particle types studied, irrespective of nature or concentration, caused considerably declined algae cell densities. The mean difference in cell density from the control, further referred to as the growth inhibition [%], increased over time,

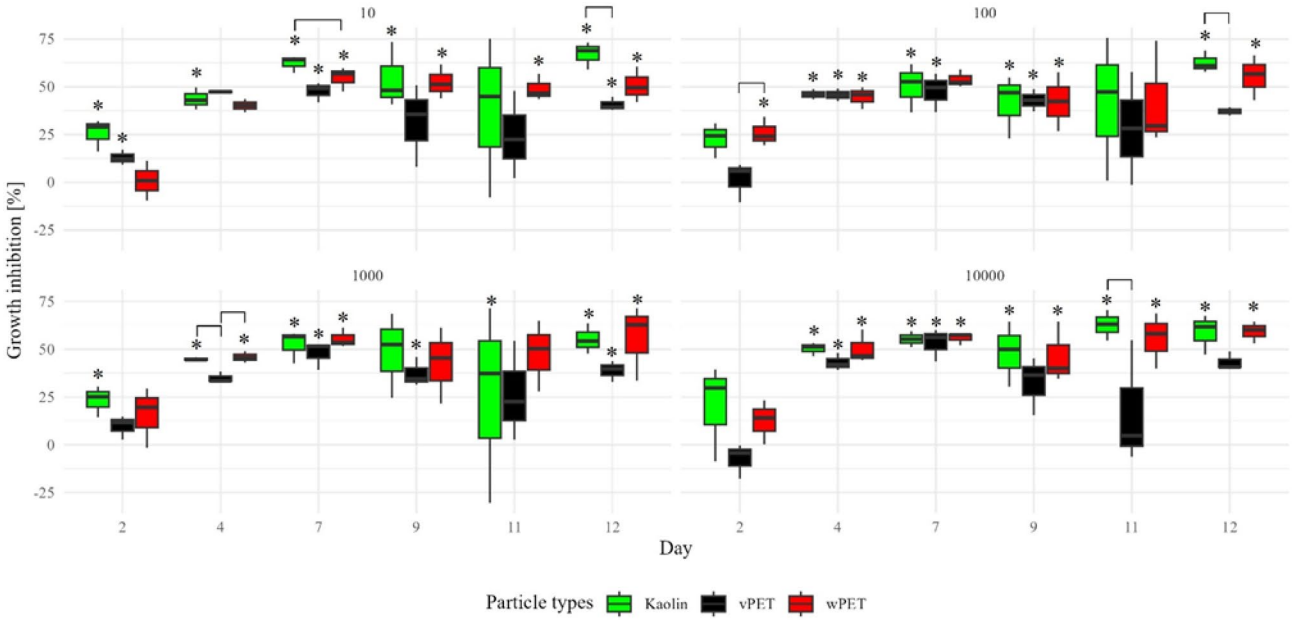

Fig. 1. Growth inhibition over the control, for the four exposure concentrations. Asterisks "*" indicate a significant difference over the control. Black lines indicate significant differences between particle types ($p < 0.05$).

reaching its plateau on day 7 (Fig. 1). Exposure to both wPET and kaolin resulted in similar inhibition patterns, causing significant inhibition from day 4 in the growth cycle, with maximum inhibition values of respectively 59.23 ± 5.73% for wPET (10000 Ps ml^{-1}, day 12) and 67.05 ± 7.25%for kaolin (10 Ps ml^{-1}, day 12). vPET however consistently caused less inhibition. Only on day 7, when the maximum inhibition of 53.32 ± 8.58% (10000 Ps ml^{-1}) was observed, all vPET exposure concentrations resulted in significant inhibitions. From day 9 onwards, the inhibition caused by vPET was lower and generally not significant. The magnitude of growth inhibition was not dependent on particle concentration. Baranyi growth models were fit to the data for analysis of the growth dynamics (SI. 9). These models captured the accumulated effects of inhibition over time in easily interpretable parameters, such as the *carrying capacity* (K), and the *maximum growth rate* (μ_{max}) of the populations. K expresses the population's cell densities at the end of the stationary growth phase and was significantly lower after particle exposure for all groups. Furthermore, the K values of the cultures exposed to kaolin were not significantly different from those exposed to wPET, however they were significantly lower than of those exposed to vPET. The maximum specific growth rate (μ_{max}) was generally not affected by exposure to the particles, except for 10 Ps ml^{-1} of kaolin, which resulted in a significantly higher μ_{max} value.

EPS production and composition

Both soluble EPS (S-EPS) and bound EPS (B-EPS) production of the algae-bacteria consortium were analysed for protein (EPS_p) and carbohydrate (EPS_c) content. Across all conditions (including the control), a significantly higher production of cellular B-EPS over S-EPS, and a significantly higher carbohydrate content (EPS_c) over protein (EPS_p) content were observed.

B-EPS$_p$

B-EPS_p production exhibited distinct patterns under different particle exposures and concentrations (Fig. 2, left). For the control, production decreased over time. However, particle-exposure led to decreased production during the exponential growth phase (day 4 – day 7), followed by increases by day 12. The increase over the control was significant on day 4 and day 12 for vPET and wPET for all concentrations. On day 12, B-EPS_p production was 165.6–208.7% higher than the control for vPET exposure, and 267.3–422.2% higher for wPET explore. These increases were noticeably higher for wPET than for vPET, though not significant ($p = 0.050$, 0.059, and 0.101 for 10, 1000, and 10000 Ps ml^{-1}, respectively). In contrast, the increases in B-EPS_p production after exposure to kaolin were only significant on day 12 for the lowest concentration.

B-EPS$_c$

The B-EPS_c production, on average factor 6.4 higher than the B-EPS_p production, also increased after particle exposure (Fig. 2, right). The increase over the control was significant on day 12 for vPET (132.4–155.1%) and wPET (168.5% – 357.1%), and was larger for wPET than for vPET – similar to the changes in B-EPS_p production - however not significant ($p = 0.050$ and 0.089 for 1000 and 100 Ps ml^{-1} on day 4, $p = 0.067$ for 10000 Ps ml^{-1} on day 12). Kaolin only caused significant increases on day 4 at 100 and 10,000 Ps ml^{-1}.No significant concentration effects were observed for vPET or kaolin, whereas wPET exposure showed a concentration-dependent increase in both B-EPS_p and B-EPS_c.

S-EPS

The production of S-EPS_p was too low to be reliably quantified. Only on day 12, the production of S-EPS_p by the control group could be reliably measured, indicating that, in contrast to B-EPS_p, exposure to the particles suppressed its production. For S-EPS_c, no data was available for day 4 due to technical issues. On day 7, S-EPS_c production after exposure to wPET and kaolin showed slight increases, significant on several instances. For vPET, production levels were comparable to the control throughout the experiment (SI. 10).

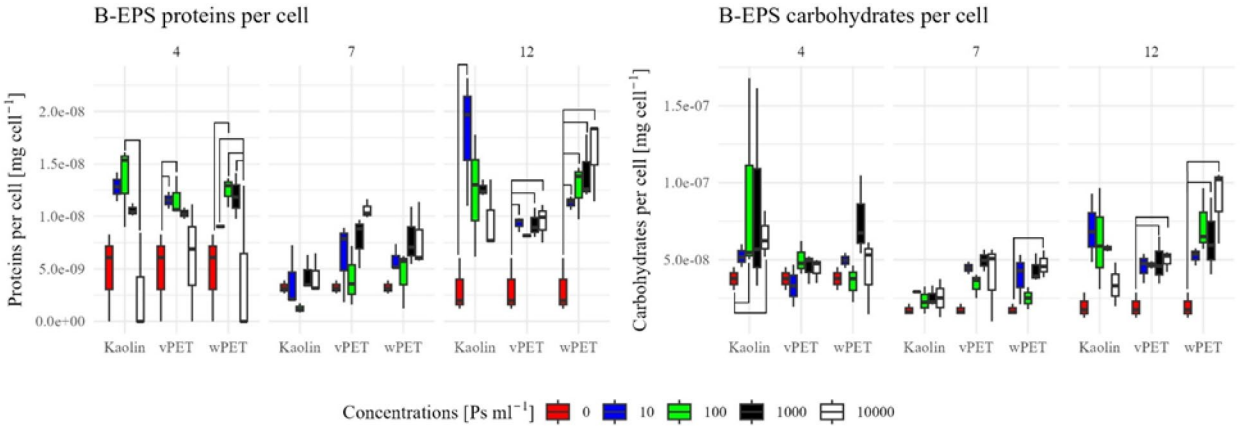

Fig. 2. Cellular bound-EPS (B-EPS) production. Left figure shows protein content, right figure shows carbohydrate content. Lines show where groups are significantly different ($p < 0.05$).

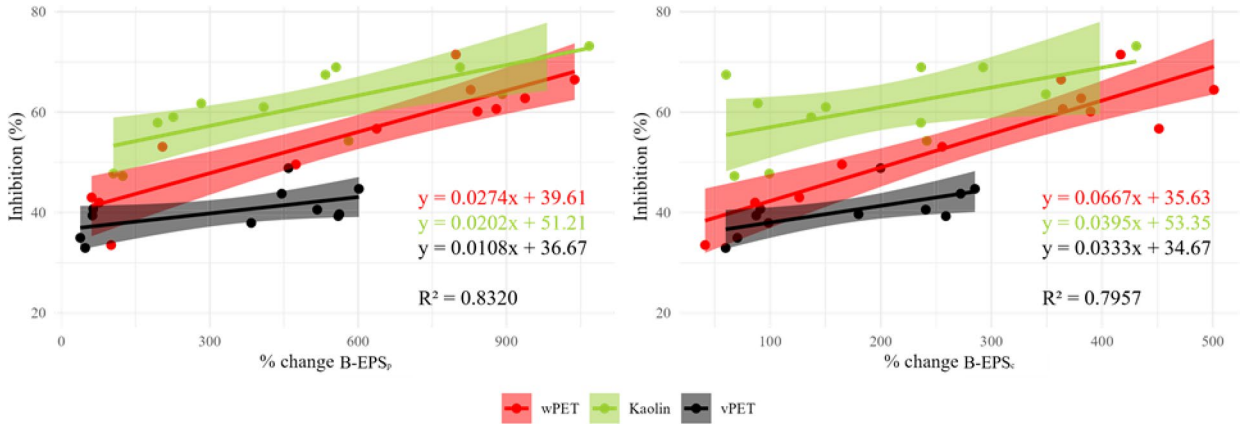

Fig. 3. Linear models assessing the relationship between growth inhibition and bound EPS (B-EPS) production, for both protein (A) and carbohydrate content (B), including interaction terms to account for differences between particle types within a single model. All models showed normally distributed residuals, with p-values < 0.05, residual standard errors (RSE) < 7.4, and adjusted R^2 values between 79% and 83%, indicating strong model fits.

	%(R4 + R8)	%R8/(R4 + R8)	%R3	%R4	%R7	%R8	%(R7 + R8)
	Aggregate to single cell ratio	Algae aggregate to total aggregate ratio	Single cell bacteria	Aggregated bacteria	Singles cell algae	Aggregates containing algae and bacteria	Algae to bacteria ratio
Control	9.42%	4.75%	87.71%	8.98%	2.86%	0.45%	3.31%
Kaolin	21.71%	1.13%	75.15%	21.46%	3.14%	0.25%	3.39%
PET	21.53%	1.16%	75.47%	21.28%	3.00%	0.25%	3.25%
wPET	22.34%	1.23%	74.05%	22.07%	3.61%	0.28%	3.89%

Table 1. Fraction of each population in the total culture (R3%, R4%, R7% and R8%), as well as derived fractions (%(R4 + R8), %R8/(R4 + R8) and %(R7 + R8).

P/C ratio

On day 12, the P/C ratio of the B-EPS had increased over the control for all particles, in all concentrations (increase over the control for vPET: 38.01 ± 9.56%; wPET: 44.98 ± 16.79% and kaolin: 73.62 ± 26.66%). The increase was only significant for 10,000 Ps ml^{-1} kaolin (SI. 10).

EPS and growth Inhibition

Linear regression analysis was performed to assess the relationship between growth inhibition (%) and change in EPS production (%) of the different EPS fractions on day 12. All models exhibited strong model fits (Fig. 3). For B-EPS$_p$, the slope, indicating the relation between growth inhibition and EPS production, was steepest for wPET (0.0274, $p = 1.75 \times 10^{-7}$), followed by kaolin (0.0202, $p = 1.90 \times 10^{-4}$) and vPET (0.0109, $p = 0.1132$). Notably, the slope for vPET was significantly lower than wPET. Similar patterns were observed for the other EPS fractions (B-EPS$_c$, S-EPS$_c$, and the P/C ratio), where EPS production correlated significantly with inhibition for wPET and kaolin, but not for vPET (slope wPET > slope kaolin > slope vPET). All model summaries are listed in the supplementary materials (SI. 11).

Aggregation

Data on the aggregation behaviour of *R. salina* and its associated bacteria upon particle exposure was collected with imaging flow cytometry (iFCM). Quantitative analysis of the bacterial community was enabled with SYBR green staining. Different populations were distinguished; population R3 are all single celled bacteria, R4 are all aggregates (length > 4 µm, width > 4 µm) consisting only of bacteria, R7 are all single celled algae and R8 are all aggregates (L > 12.5 µm, W > 20 µm) consisting of at least one algae cell, possibly including bacteria as well.

Aggregation

Looking at the fractions each population represents, as listed in Table 1, several observations were made.

An increase in total amount of aggregates (R4 + R8) was observed after exposure, going from 9.42% in the control group to values of 21.53–22.34%. This increase in aggregation was moderately correlated with overall EPS production ($r = 0.646$, $p < 0.05$). When split by exposure type, this correlation was strongest under vPET ($r = 0.847$, $p < 0.05$) and wPET ($r = 0.734$, $p < 0.05$) exposure, but weaker and not statistically significant under kaolin ($r = 0.505$, $p = 0.0546$), indicating an exposure-dependent link between aggregation and EPS. Interestingly,

the increased aggregation was carried by an increase in percentage of bacterial (R4) aggregates, while the total percentage of algae aggregates (R8) decreases, dropping from 4.75% in the control to 1.13–1.23% in exposed groups. The shift to a lower representation of algal aggregates (R8) in the total number of aggregates formed (R4 + R8) was remarkable, given that the relative algal abundance (%(R7 + R8)) remains stable across all conditions (3.25–3.89%).

Size distribution

Across all treatments—regardless of particle type, weathering state, or concentration—particle exposure led to a significant reduction in algae single cell size. Exposed algae cells were on average 4.51 ± 1.07% smaller (97.9 ± 1.1 μm²) compared to algae cells in the control group (102.5 ± 8.7 μm²). This decreased cell size was strongly correlated (r = -0.811, $p < 0.05$) with the observed growth inhibition, for all three particle types (Fig. 4).

Furthermore, despite reduced frequency of aggregating, R8 aggregates (containing algae) show a shift to forming larger aggregates after exposure. Mean aggregate area was smallest in the control (149.7 ± 1.6 μm²), and significantly higher after exposure to kaolin (179.9 ± 4.5 μm²) and wPET (159.9 ± 1.6 μm²). Kaolin aggregates were significantly larger than vPET and wPET aggregates. However, the median lengths are highly similar across all groups, indicating that the differences are primarily driven by an increased number of larger aggregates in the exposed groups. This was supported by the interquartile range (IQR) and standard deviation (Std Dev) values of the size distributions. The IQR was broader than the control (38.2 μm²) for kaolin (48.2 μm², $p < 0.05$), wPET (46.4 μm², $p < 0.05$) and vPET (43.9 μm²). Additionally, all the exposed groups have significantly higher Std Devs then the control (41.7 μm²); kaolin (189.1 μm²), wPET (134.9 μm²), vPET (141.5 μm²). To identify exceptionally large aggregates, the proportion of aggregates exceeding the 90th percentile threshold of the control group (196.1 μm²) was calculated. All exposure groups showed a higher proportion of large aggregates: kaolin had the highest percentage of large aggregates (16.2%, $p < 0.05$), followed by wPET (14.3%, $p < 0.05$) and vPET (11.1%), confirming that exposure, specifically to kaolin and wPET, promotes the formation of larger aggregates.

For population R4 (purely bacterial aggregates), increases in aggregate size simultaneous with the increase in aggregating frequency were observed. In the control, the aggregates had a mean area of 10.84 ± 2.41 μm², while after exposure, aggregates had mean areas of 14.87 ± 0.33 μm² (kaolin), 15.36 ± 0.53 μm² (vPET) and 15.80 ± 0.59 μm² (wPET), indicating increased bacterial aggregation, independent of the particle type. However, both the IQR (8.17–8.25 μm²) and the Std Dev values (15.4–25.2 μm²) did not significantly differ from the control. To identify exceptionally large aggregates, the proportion of aggregates exceeding the 90th percentile threshold of the control group (20 μm²) was calculated. wPET had the highest percentage of large aggregates (17.56%), followed by vPET (16.47%) and kaolin (16.07%), all significantly higher than the control.

The results highlight how population R4 and population R8 have different responses in terms of aggregation behaviour after exposure to particles. In R8, the shift in mean size without a change in median, combined with increased variability, indicate a more asymmetric distribution with a right-skewed tail, implying that more extremely large aggregates have emerged after exposure. In contrast, the consistent increases in both mean and median sizes for R4, with unchanged variability, point to a more uniform shift across the entire population.

Interestingly, linear regression analysis indicated strong correlations between R8 aggregate sizes and both B-EPS$_p$ and B-EPS$_c$ production for all particle types. However, for R4 aggregate sizes the correlation with B-EPS$_{c\ was}$ significant, but not with B-EPS$_p$. These relations were not particle-type dependent, suggesting a

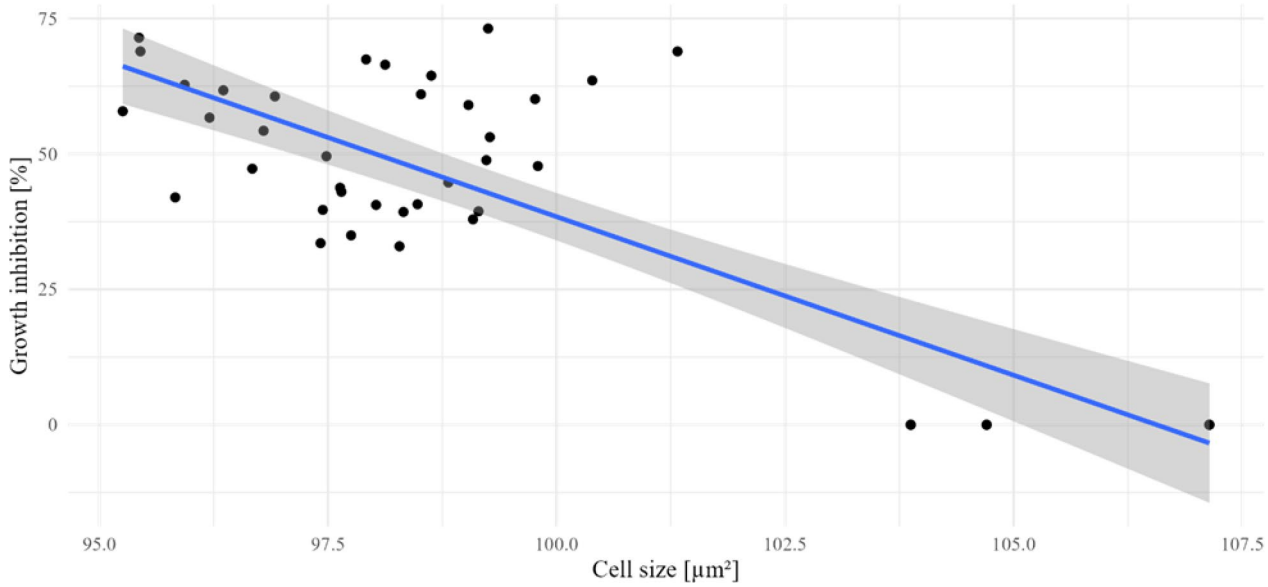

Fig. 4. Correlation between growth inhibition and cell size. vPET (-0.922, $p < 0.05$), wPET (-0.844, $p < 0.05$) and kaolin (-0.787, $p < 0.05$). Correlation independent of particle type.

general link between EPS and aggregate size. Full model results are provided in the supplementary materials (SI. 12).

Aggregate composition

To better understand these changes, the composition of the different aggregates was examined. The R4 aggregates, consisting exclusively of bacteria, are further referred to as "B" aggregates. The R8 aggregates with only algae are referred to as "A" aggregates, while the R8 aggregates with both algae and bacteria as "AB" aggregates. In the B aggregates, the average number of bacteria per aggregate was not significantly different from the control after exposure. An interesting shift was observed in the R8 aggregates after exposure to the particles. In the control group, 36.10% of the aggregates are pure algal aggregates. However, upon exposure, this number goes down to 26.62–26.99%, indicating that 73.01–73.38% of the aggregates contains both algae and bacteria. In the control group, AB aggregates contained on average 2.3 bacteria per aggregate, whereas after exposure this number significantly increased to 4.5–5.5 bacteria per aggregate (Fig. 5). The number of algae per aggregate within the AB aggregates remained stable, similar to the number of algae cells per aggregate in the A aggregates.

Discussion

This research examined the effects of microparticle exposure on the algae species *R. salina*, in association with bacteria. Algae specific endpoints (algae growth dynamics) were analysed, as well as emergent end-points of the consortium (EPS production and aggregation formation), comparing virgin versus weathered particles, as well as plastic versus a natural particle. Emergent responses of the consortium were assessed, as they reflect the responses of a more ecologically relevant scenario. The results reveal distinct response-profiles; wPET and kaolin exhibit similar profiles, characterised by strong and persistent algae growth inhibition, significantly correlated to increased B-EPS production, indicating a coordinated stress response. Additionally, the significant increase in aggregate number and size was significantly correlated with the elevated EPS production. The similar response-profiles of wPET and kaolin are contrasted by the response-profile of vPET, which was in general much less outspoken, and most importantly, does not show a correlation between growth inhibition and the production of EPS, indicating a generic rather than a coordinated stress response. Nevertheless, increases in aggregate number and size were observed, which—similarly to the other particle types—were correlated with the level of EPS produced, further highlighting the role of EPS in mediating aggregation, even under mild stress conditions. Furthermore, significant decreases in algae cell size (area) were observed after particle exposure. Finkel et al., (2007) show that a lower metabolic rate, related to lower population size, corresponds to lower cell sizes[48,49]. This was in agreement with our observations, where the cell sizes in the populations exposed to particles were significantly lower.

ATR-FTIR spectra and DLS data, reported in the *material and methods* section, elucidate hidden aspects of the particles surface characteristics and stability in the medium. As such, these data may help understand differences in stress profiles between the virgin and weathered plastics. The vPET and wPET are both PET plastics with similar average diameters (710 nm and 740 nm) and were dosed in the same concentration (10–10000 Ps ml^{-1}). Controls were used to account for the surfactant DPPC in the vPET reference sample, nonetheless, differences in the effects were observed. Possible explanations for the difference in stress profiles were either enhanced additive/contaminant leaching due to weathering[50,51] and/or changes in particle surface characteristics after weathering. Previous work by the same authors (Sioen et al., 2024) includes a detailed exposure assessment of acetaldehyde leaching from PET[32] demonstrating that even under conservative worst-case assumptions, the

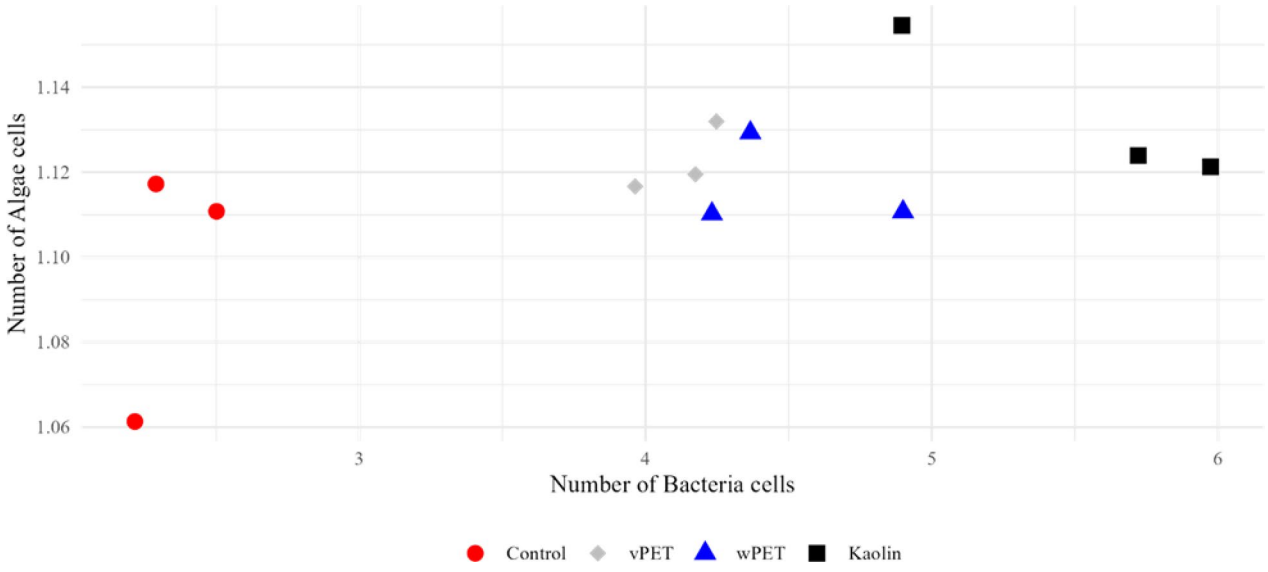

Fig. 5. Composition of AB aggregates; aggregates containing both algae cells and bacteria cells, after exposure to particles.

resulting concentrations in the test medium remain several orders of magnitude (factors to over 10^7) below known toxicity thresholds for microalgae[52–54]. These findings, together with ecotoxicological studies that found no adverse effects of PET leachates on algal growth[55] suggest that leachates are highly unlikely to account for the observed toxicity differences between virgin and weathered particles in our experiments.

However, ATR-FTIR spectra and DLS data provided information on the particles surface characteristics and stability in the medium. The infrared spectra enabled us to determine the carbonyl index (CI) of both plastic samples. The CI was commonly used to assess the degree of oxidation in polymers by quantifying changes in the carbonyl vibrational band[56,57]. Specifically, it was calculated as the ratio of the integrated surface area of the carbonyl peak (at 1730 cm^{-1}) to that of a reference peak (at 720 cm^{-1}). This ratio increases with increasing oxidation due to polymer degradation progresses[58]. In this study, the measured CI of virgin PET (vPET) was 0.95 ± 0.03, whereas the CI of weathered PET (wPET) was significantly higher at 1.15 ± 0.02. This increase suggests a greater degree of surface oxidation in wPET, likely resulting from the formation of carboxylic (COO^-) groups. The presence of such polar functional groups increases surface hydrophilicity. ICP-MS analysis of both vPET and wPET, performed by the manufacturer (JRC), confirmed an elevated presence of surface-bound COO^- groups on the weathered particles[40]. In addition, the JRC's measurements of the hydrophobicity index showed a significant shift in values from -0.12 ± 0.06 for vPET to -1.61 ± 0.21 for wPET. According to OECD Guideline 126, values below -1 are indicative of hydrophilic behaviour, which further supports the conclusion that environmental weathering increases the hydrophilicity of PET particles[40,59]. These findings were further supported by the dynamic light scattering (DLS) measurements. The hydrodynamic diameter (HD) of wPET was significantly smaller than that of vPET (176.97 ± 22.72 nm vs. 719.83 ± 44.83 nm), suggesting that weathered particles were less prone to aggregation. The increased surface charge (due to the presence of more COO^- groups) contributes to enhanced colloidal stability and better dispersion of the particles in the water column. This was also reflected in the zeta potential measurements: wPET exhibited a more negative zeta potential (-20.77 ± 1.84 mV) compared to vPET (-17.93 ± 0.74 mV), indicating a higher degree of electrostatic repulsion and, consequently, improved suspension stability. Altogether, these results demonstrate that weathering of PET leads to particles with greater surface oxidation, increased hydrophilicity, and enhanced colloidal stability[60]. From an ecotoxicological perspective, such physicochemical changes likely result in a higher bioavailability of weathered particles, as they remain longer in suspension and are more in interaction with algae cells[61]. These mechanisms offer a plausible explanation for the lower toxicity observed following exposure to vPET particles compared to the increased toxic response observed with wPET. This was in line with previous observations, such as those of Ni et al., (2023), who observed higher toxicity for aged PS (0.1–10 µm, 1–50 mg L^{-1} ~ 1.91×10^3–9.55×10^{10} Ps ml^{-1})[42] as well as Wang et al., (2020) for aged PVC (50–100 µm, 10–200 mg L^{-1} ~ $13.1–2.09 \times 10^3$)[62]. Even though it is outside the scope of this research project, it is important to note that while particles alter the biological system, the biological system will also alter the particles. Research has demonstrated that the presence of natural organic matter (such as EPS) further improves plastic stability due to the steric repulsion[63]. Consequently, the production of EPS as a stress response could trigger a feedback loop, further aggravating particles' toxicity due to increased stability and thus bio-availability. While this mechanism requires further investigation, our observations of both higher EPS production and growth inhibition in wPET-exposed samples support this hypothesis. Environmental plastics inevitably undergo weathering, leading to altered stability, fate and toxicity compared to virgin polymers[64]. The inclusion of a weathered control in MNP toxicity assessments is thus essential for drawing robust and environmentally relevant conclusions[60].

Interestingly, the stress profile of wPET was not very different from kaolin - a naturally occurring particle. Briefly, wPET and kaolin particles had similar average diameters (740 nm and 830 nm) and were dosed in the same concentrations (10–10000 Ps ml^{-1}). The DLS measurements show that kaolin has a slightly more negative ZP (-29.93 ± 0.56 mV) than wPET (-20.77 ± 1.84 mV), indicating higher particle stability in the water. On the other hand, kaolin has a higher HD (486.6 ± 15.56 nm) than wPET (176.97 ± 22.72), suggesting that more aggregation may have occurred in kaolin suspensions, despite its higher electrostatic stability. These seemingly contradicting observations can be explained by their different aggregation mechanisms. Kaolin particles are platelets, with three distinct surfaces; a silica face, an alumina face (both negatively charged) and the edge, either negatively or positively charged. The stability of the particles is dependent on complex face-to-face and edge-to-face interactions of the kaolin particles[65,66]. On the other hand, interactions by wPET particles are determined by steric stabilization, promoted by the presence of the surface-bound carboxyl groups that form hydrated shells around the particles, thereby reducing particle-particle interactions and preventing aggregation[67]. These different interaction mechanisms explain why kaolin, despite the more negative ZP, has a higher tendency to form aggregates. Although the aggregation mechanisms differ between the two particle types, their characteristics—moderately negative ZP's and relatively small HD's—both indicate low tendencies for aggregation. These similar characteristics of kaolin and wPET lead us to assume that the observed toxicological effects may be attributed to generic particle interactions with algal cells, rather than to material-specific chemical toxicity. Additionally, even though both wPET and kaolin induced similar stress response profiles, it cannot be excluded that specific properties of EPS productions, including stickiness, may have been differently altered as a stress response and may in turn lead to changes in aggregation. Only two studies on MNP toxicity towards microalgae have included natural particle controls in addition to our own previous work[32]. Gorokhova et al., (2020) exposed *Raphidocelis subcapitata* (a freshwater species) to kaolin, wPET and vPET (11 and 12 µm, 10–1000 mg l^{-1} ~ 8×10^3– 10^6 Ps ml^{-1}), and observed growth inhibition, with no significant differences in effects between plastics and kaolin[43]. Cheng et al., (2024) exposed *Chlorella vulgaris* to PET, PP and cotton fibres (0.01–100 mg l^{-1}, no size data), and observed higher inhibition for the synthetic fragments[68]. Expanding the scope, four publications compared the effects of natural and synthetic particles on *Daphnia magna*. These produce conflicting outcomes, ranging from no toxic effects of natural particles[69] to higher toxicity compared to synthetic particles[70]. However,

straightforward comparison of effects among research is complicated, due to the high heterogeneity in particle type, shape, size and concentrations, as well as the large variation in test-organisms.

Among other functionalities, EPS production has been described as a microbial stress response, exhibiting a protective function. Su et al., (2025) observed that removal of EPS weakened algae ability to deal with nanoplastics stress[71]. Defence mechanisms, such as EPS production, inherently involve trade-offs that balance protection and physiological performance[72]. For example, the energy allocated to the production of EPS, was no longer available for cellular growth and division. This metabolic cost likely explains the observed decreased growth after particle exposure[72,73]. Additionally, as EPS are also produced by bacteria, it cannot be excluded that the EPS was a also produced as a bacterial stress response[6]. The data demonstrate that particle exposure, regardless of type or concentration, significantly alters aggregation dynamics. The total number of aggregates formed, pure bacterial aggregates (R4) and aggregates including algae cells (R8), significantly increased and was significantly correlated with the B-EPS produced. Next to the increased number of aggregates, shifts in aggregate size were observed. The aggregates formed were significantly larger and more variable in size compared to the control. Interestingly, significant correlations between B-EPS production and aggregate sizes were observed. Moreover, not only the quantity, but also the composition of EPS affects aggregation dynamics. Protein-rich EPS, indicated by a higher P/C ratio, tends to be more hydrophobic and adhesive, promoting aggregate formation, as reported in previous studies[74,75]. This was supported by our observations, where on day 12, exposure to particles consistently lead to higher P/C ratio's, aligning with the observed increase in aggregate sizes. EPS serves its protective function by creating a protective barrier around the cell, hindering contact with toxicants[13]. However, this barrier also hinders the passage of light, and the diffusion of nutrients and gasses. This trade-off between the cellular defence mechanism, and the simultaneous hindrance of efficient photosynthesis, likely explained the observed coupling between EPS production and growth inhibition. Also, the sticky nature, as indicated by the higher P/C ratio, of EPS facilitates the formation of larger algae aggregates, as was observed in these experiments. Aggregation as a defence mechanism reduces the contact area of cells with external substances, such as toxicants. Again, this is a trade off with passage of light and substances for sustained cell growth[76,77]. Zhang et al., (2023) provided supporting evidence for the algal defence mechanism, identifying EPS production as a key metabolic strategy against perchlorate stress through multi-omics analysis, and observed reduced growth and photosynthesis in combination with EPS production and increased aggregation[77].

Microbial aggregation is a crucial process in maintaining stable marine ecosystems. Marine snow, transporting carbon and nutrients through the water column, consists mainly of microbial aggregates[78]. The role of bacteria in marine snow formation has long been underestimated, however is gaining wider recognition[79]. In the algae-bacteria associations, interactions occur on the surface of algae cells, the so-called phycosphere, as it is rich in algae-exuded molecules[80]. These algal exudates, such as EPS, promote algal-bacterial aggregation, and stimulate bacterial EPS production, thereby creating joint extracellular matrices[6].

In summary, this study provides a system-level view of microbial community dynamics under MNP exposure, which is valuable because microbial interactions—rather than the behaviour of individual species—shape ecosystem function[5]. While the bacterial composition in this experimental work were controlled nor identified, all experimental groups originated from the same initial culture, ensuring that any observed differences emerged during the experiment. Although causality cannot be inferred, analysing these patterns enhances our understanding of microbial ecosystem responses to environmental stressors. In future studies, community profiling of the consortium (e.g. with 16 S rRNA sequencing) could shed light on shifts in community composition after MNP exposure. As both increased aggregation and simultaneous algae growth inhibition were observed, which have conflicting consequences for vertical carbon transport, drawing straightforward conclusions from this research on the cumulative impact of MNPs on marine carbon transport is complicated. No empirical quantification was done in this work that allows for drawing conclusions on the effects of MNPs on the cumulative marine carbon transport. Modelling approaches would offer opportunities, however would require additional data on the effects of zooplankton grazing on algae, as well as effects of altered aggregation patterns on zooplankton[81].

Conclusion

This study demonstrates that algal aggregation and EPS dynamics in the algae-bacteria consortium of *R. salina* in response to micro- and natural particles is rather shaped by particle properties such as surface chemistry and hydrophilicity than by their origin (synthetic or natural). Weathered PET and kaolin induced stronger and more coordinated responses than virgin PET, as evidenced by persistent growth inhibition, increased EPS production, and the formation of more and larger aggregates. These responses suggest that EPS is produced as a protective mechanism, creating a protective layer and promoting aggregation. This response is an assumed trade-off for metabolic energy, thereby explaining the observed growth inhibition. By integrating weathered and natural particle controls, this work offers an ecologically grounded perspective on microplastic toxicity. Furthermore, these findings highlight the importance of studying microbial consortia and emergent properties, next to single-species growth assays, reflecting environmentally relevant experimental conditions. Future regulatory assessments and ecosystem models should account for such complexity to better predict the ecological consequences of micro- and nanoplastic pollution.

Materials and methods

To ensure high quality experimental work, and reproducibility of the work, the experiment was designed following the guidelines proposed by De Ruijter et al. (2020) for microplastic effect studies. These guidelines were designed in order to standardize the testing of effects of MPs in aquatic test systems, and relate to the technical quality of the tests and their applicability in risk assessment[82] .

Microalgae culture

The micro-algae culture used for the experiments was *Rhodomonas salina*, a brackish marine algae species. The culture was obtained in 2016 from CCAP (Culture Collection of Alae & Protozoan) and has ever since been maintained in the Blue Growth Research Lab, at the Department of Animal Sciences and Aquatic Ecology of Ghent University. The algae were cultured in L1-medium as described by Guillard and Hargraves[83] made with filtered (0.22 µm) natural seawater (SEA LIFE, Bredene) with a salinity of 24‰. Four days before the start of each experiment, a new algae culture was set-up, with an initial algae cell density of 10^5 cells ml^{-1}. The cultures were maintained in a temperature-controlled room (20.1 ± 0.25 °C), with a light dark regime of 16:8 h, at an intensity of 2500 lx (Phillips GreenPower LED, GPL PM 210 DRBFR L240 G3.0 C3; 58.9% blue, 25.7% green, 12.8% red, 2.6% far red) for the entire duration of the experiments[84].

Particle types

Particles

The effects of two types of plastic particles and a natural particle were assessed, all fragmented, polydisperse and with a maximum diameter of 5 µm. The MNPs were virgin polyethylene terephthalate (vPET) and chemically weathered PET (wPET), both manufactured by the Joint Research Centre of the European Commission (EC JRC, Geel)[40] and the natural particle kaolin (Imerys, Polwhite E). The JRC manufactured the PET MNPs using PET powder from Goodfellow (Goodfellow, Cambridge, UK, Lot No. 300830480). The vPET MNPs were stored in a 0.1% DPPC (dipalmitoylphosphatidylcholine) solution, to reduce the particles' hydrophobicity and as such increase their stability. The vPET was weathered by the JRC by means of alkaline hydrolysis. For this, the vPET powderwas treated with KOH (potassium hydroxide), followed by an ultrasonic treatment. This process introduced COO^-- groups to the polymer chain, increasing its hydrophilicity, allowing the storage of wPET in pure DI without surfactant[40]. In terms of additives, the PET MNPs were derived from PET that contains one ppm of acetaldehyde. This is far below the reported toxicity values for marine microalgae of 237–459 ppm (120-hour EC_{50} for *Nitzschia linearis*) and 23 ppm (2-hour EC_5 for *Chlamydomonas reinhardtii*)[52–54]. A more detailed analysis of the additives and implications is included in the Supplementary Materials (SI. 2). The natural particle kaolin was also stored in pure deionized water (DI) without surfactant. All particle stocks were filtered over a 5 µm pore size filter (Whatman, cellulose nitrate, AE98 10400212) to exclude the larger particles.

Particle characteristics

Particle characterisation was done in terms of size, shape, type and source of the particles. All characterisation is reported in this text, and in the supplementary materials, as was recommended by De Ruijter et al., (2020) in their guidelines for microplastic effect studies[82]. The concentration and particle size distribution of the plastic and kaolin stock suspensions were determined with the ClassizerONE (S1.4.34, EOS) by JRC (Ispra, Italy). The stocks have respective suspension concentrations of 10^7, 1.2×10^6 and 1.7×10^7 Ps ml^{-1} for vPET, wPET and kaolin, with respective average diameters D_{av} of 710 nm (D_{10} = 580 nm, D_{90} = 810 nm), 740 nm (D_{10} = 450 nm, D_{90} = 1020 nm), and 830 nm (D_{10} = 630 nm, D_{90} = 970 nm) (SI. 3). ATR-FTIR analysis was used for chemical characterisation of the surface groups (Nicolet iN10 MX). To collect the particles from the liquid, 3 ml of the particle suspension was filtered over a 200 nm filter, after which the filter was dried in a 60 °C oven. The residue was scraped of the filter for identification and analysis using FTIR spectroscopy. The obtained FTIR spectrum of the PET particles matched spectra reported in literature, with characteristic peaks at 3100 –2800 cm^{-1} (aromatic and aliphatic -C-H bond stretching), 1720 cm^{-1} (ester carbonyl bond stretching), 1300 cm^{-1} (ester group stretching) and 1100 cm^{-1} (methylene group), confirming the particles polymer type[85]. The carbonyl index's (CI) of vPET and wPET, calculated from the peak areas of the carbonyl group (1713 cm^{-1}) and the aromatic rings (722 cm^{-1}), were respectively 0.95 ± 0.03 and 1.15 ± 0.02 (student's t-test; $p = 0.00155$) indicating an increased presence of COO^--groups and thus oxidation after weathering (SI. 5). Scanning Electron Microscopy (SEM) images were collected for visual confirmation of the particles fragmented shapes. For this, droplets of particle suspension were put on carbon stickers, and were dried in the oven (60 °C), after which the samples were loaded into the SEM (Phenom ProX) with a backscattered electron detector (SI. 6). The zeta potential (ZP) and electrophoretic mobility (EM) of the three particles in L1-medium were measured by means of Dynamic Light Scattering (DLS) with a Zetasizer ver. 7.11 (Malvern Instruments, using a clear disposable zeta cell). wPET, vPET and kaolin have respective ZP values of -17.93 mV, -20.77 mV and – 29.056 mV, and EM values of -1.27 µmcm Vs^{-1}, -1.47 µmcm Vs^{-1} and 2.12 µmcm Vs^{-1} (SI. 7).

Experimental design

This experimental design is similar to what is described in previously published work, and was based on the OECD guidelines of toxicity testing with microalgae, but adapted for long-term experiments as recommended by De Ruijter et al., (2020)[32,82,86]. The algae *R. salina* were exposed to the three particle types (virgin PET (vPET), weathered PET (wPET) and kaolin) separately, with concentrations of 10, 100, 1000 and 10,000 Ps ml^{-1}, for 12 days, covering their growth curve (timeframe based on previous observations). The particle concentrations were derived from the measured average environmental MP concentration in the North Sea, the Artic and the Baltic Sea of 0.058 MP m^{-3} (2.75 mm), as described in literature[38]. Assuming the complete degradation of a 2750 µm PET particle to MNPs with a SD similar to those of the particles used in these experiments, the environmental MP concentration was converted to the assumed MNP concentrations (SI. 4). This method is based on mass conservation principles as proposed by Besseling et al., 2019 [37]. During the experiment, the well-plates were placed on a lightbox (Phillips GreenPower LED, GPL PM 210 DRBFR L240 G3.0 C3; 2500 lx; 58.9% blue, 25.7% green, 12.8% red, 2.6% far red) in a temperature controlled (20.1 °C ± 0.25 °C) culture room and a light dark regime of 16:8.

The experiment exposed algae to a concentration range of different particles. A negative control without particle exposure is incorporated, along with a control containing particles without algae. Each treatment is conducted in triplicate. Since EPS is analysed at three time points during the growth curve (days 4, 7, and 12), and for the analysis of EPS the entire culture is collected, the entire experimental setup as described is replicated three times for each time point (3 × 3). The experiment is executed in 6-well plates (polystyrene, VWR International). Before the start of the experiment, the particles were washed three times through centrifugation (2500 rpm, 5 min, 18 °C), with replacement of the supernatant suspension liquid with L1-medium. The particle concentration series is made through serial dilution with the L1-medium. Algae cultures, set up four days before the start of the experiment, were transferred to volumetric flasks, with an initial cell density of 10^4 cells ml^{-1}, after which the particles were transferred to reach the desired exposure concentration. For the untreated negative control, L1-medium without particles was added. For the particle controls without algae, only L1-medium was brought into the volumetric flask, after which the particles were added. Filter sterilized (0.20 µm) DPPC was added to each group to level the DPPC concentration in the treatment with 10,000 Ps ml^{-1} of vPET (10^{-7}%). This initial set-up in volumetric flasks was to ensure homogenisation of the algae and particle concentrations over the different wells. Next, the algae-particle mixtures were transferred to the 6-well plates (9 ml per well) and randomly placed on the light-box. The well-plates were carefully shaken daily (4s) to facilitate mixing of the algae and the particles.

Measurements

Algae cell density, temperature and pH were measured on days 0, 2, 4, 7, 9, 11 and 12. EPS was measured on day 4, 7 and 12. Aggregation was analysed on day 10.

Temperature and pH.

Temperature is measured with a thermostat with interface (VWR 61161-378). pH is measured with a pH-probe (Consort, P407).

Algal cell density

Algal cell density was measured by means of flow cytometry, using a Beckman CytoFLEX instrument equipped with CytExpert software (version 2.6.0.105). Calibration was conducted before measurements using CytoFLEX Daily Fluorospheres (B53230). The flow cytometer was configured with the FSC detector (gain: 165) and the FITC fluorescence detector (emission at ~ 520 nm, gain: 240). Samples were analysed at a flow rate of 30 µl min^{-1}, with stopping criteria set to either 10,000 events or 60 s of acquisition. To identify and quantify the algal population, a gating strategy was applied based on autofluorescence (peak at 540 nm) and forward scatter characteristics. A histogram of FITC fluorescence intensity of each object passing was constructed, and a gate was set to include events with autofluorescence consistent with *R. salina*. The gated population was further validated based on forward scatter (FSC) properties, confirming the expected size distribution for *R. salina*. For background correction, pure L1-medium and L1-medium containing particles were analysed to account for potential interference from medium components.

EPS production

Both soluble EPS (S-EPS) and bound EPS (B-EPS) were extracted from the algae samples. The protein and carbohydrate content of both fractions was determined. The B-EPS was extracted using the heat-ultrasonic extraction method and is described in detail in previously published work[32,87]. The supernatant after the first centrifugation step is used for further analysis, as it contains the S-EPS[88,89]. The protein content was determined by adding 250 µl Bradford Reagents to 25 µl of sample. Following incubation (5 min), the optical density (absorbance) of each sample was measured at 595 nm, using a spectrometer (Thermo Labsystems, Multiskan Ascent), which correlates to the amount of proteins in the sample[90]. The carbohydrate content was determined using the Phenol-Sulphuric Acid Method. For this, 40 µl of a 20% phenol solution is added to 400 µl of sample[91]. Next, 1 ml of sulphuric-acid is added to dehydrate the carbohydrates and form furfural derivatives. These derivates then react with the phenol and form coloured stable bindings. The optical density is measured at 490 nm. The colour changes were converted to concentrations by means of previously built calibration curves. To account for variation in biomass across treatments, EPS production was normalized to algal cell density. Although EPS is produced by both algae and associated bacteria, algal cells are the primary structural units of the consortium and represent the most consistent and quantifiable biological component. This normalization allows for comparative interpretation of EPS production relative to the algal host, acknowledging that measured EPS is a property of the entire consortium.

Aggregation

Subsamples were transferred to 1.5 ml Eppendorf tubes, stained with a SYBR® Green I nucleic acid gel stain (cat. no. S7563; Invitrogen; Thermo Fisher Scientific, USA) [working solution: 1:100 in DMSO (cat. no. D4540; Sigma-Aldrich; Merck KGaA, Germany), final stain concentration: 1:10000], incubated for 20 min at 21 °C in the dark, and analysed using the ImageStream®XMk II (Amnis part of Luminex, Austin, Texas, USA).

The template to acquire the data with the image flow cytometer was set as follows: per object, one bright field image (LED, 14.40 mW) was captured on Ch01 and the SYBR Green I signal on Ch02 (488 nm, 0.5 mW) of the first CCD camera, while the second bright field image (LED, 10.72 mW) was captured on Ch09 and the auto-fluorescent signal on Ch011 (642 nm, 0.5 mW) of the second CCD camera. The dark field (SSC, 785 nm, 3.44 mW) images were not retained for further analysis. Data acquisition ended when 5000 objects (within a predefined 2D region: x-axis [intensity Ch02: -450–1e07] and Y-axis [intensity Ch011: 1e04–2e07]) were measured or when a time of 5 min had passed. All images were captured with the instrument-specific Inspire

Region	Objects	Intensity Ch011	Width (µm)	Length (µm)
R3	Non-attached bacteria	0–50,000	0–4	0–4
R4	Aggregates including bacteria only	0–50,000	>4	>4
R7	Single celled *R. salina*	>50,000	6–12.5	0–20
R8	Aggregates including *R. salina* cells and bacteria	>50,000	>12.5	>20

Table 2. Parameter values for the template of the iFCM data analysis. To determine the amount of bacteria in R4 and the amount of bacteria and algal cells in R8, Ch02 and Ch011 *.tif images of the objects in both regions were exported using the Ideas software (v.6.2.187.0) and subsequently analysed applying a custom made macro in ImageJ (v1.54 m, https://imagej.net/ij).

y	Cell density at certain time point	cells ml^{-1}
y_0	Initial value of abundance or cell density	cells ml^{-1}
μ_{max}	Maximum growth rate	$time^{-1}$
K	Carrying capacity (max abundance or cell density)	cells ml^{-1}
h_0	Parameter specifying the initial physiological state of organisms, $h_0 = \mu_{max} * \lambda$, with λ the length of the lag phase	$time^{-1}$

Table 3. Baranyi growth model parameters. The growth model parameters for each particle type and concentration were compared by means of one-way ANOVA for normally distributed data, and the non-parametric Kruskal-Wallis test for the data not meeting the assumption of normality. Tukey and Dunn post-hoc tests were performed in case of p-values < 0.05, for respectively normal and non-normal distributed data.

software (v.201.1.0.765) and processed with the Ideas software (v.6.2.187.0). A single template created with the latter software was used to analyse all subsamples and to determine the amount (count, objects/ml), length, width, and area of respectively non-attached bacteria (R3), aggregates including bacteria only (R4), single celled *R. salina* (R7), and aggregates including *R. salina* cells and bacteria (R8). The values of the parameters on which the template is based can be found in Table 2.

Data analysis

The data collected for the different end-points (cell density, EPS and aggregation) were analysed in relation to the particle types and concentrations, using R software (RStudio 2023.12.1 Build 402). Growth inhibition [%] was calculated as the percentual difference in density from the control. Consequently, the statistical significance of the measured differences was evaluated for all end-points. The criteria of normality and homogeneity of variance were tested with Shapiro's and Levene's test. For comparison with the control, either a parametric t-test or a non-parametric Wilcox test was used. When comparing different concentrations within a single particle type, or comparing different particle types within a single concentration, either parametric one-way-ANOVA and Tukey's HSD post-hoc tests, or the non-parametric Kruskall-Wallis test and Dunn's post-hoc test were. Analysis of the growth cycle was performed by means of growth-model analysis (see below).

To analyse the relationship between different end-points (inhibition and EPS production, EPS production and aggregation, inhibition and aggregation), correlation analysis was performed using Pearson correlation coefficients. Linear regression models were constructed to evaluate the influence of particle type on these relationships, including interaction terms to test for differential effects. Model assumptions were checked by assessing residual normality, and model fit was evaluated using adjusted R^2 and residual standard error.

Growth model analysis

The cell-density data was used to fit growth-models, using the R package *growthrates* (version 0.8.4). Different parametric models were optimized by means of *ordinary least squares (OLS) regression*, and their model fits were assessed with model-fit indicators (R^2 maximized and *RRS* minimized). For the nonlinear regression, a set of initial parameters was chosen based on the experimental data, together with box-constraints to prevent unrealistic parameter values. An iterative approach was used, where models were re-fitted with the estimated coefficients from the previous fitting as start-parameters, until the model-fit indicators no longer improved. The optimal growth-model was the Baranyi parametric model, with an equation of following form:

$$log\,(y) = log\,(y_0) + A * \mu_{max} - log(1 + \frac{exp\,(\mu_{max} * A) - 1}{exp\,(log\,(K) - log\,(y_0))}) \quad (1)$$

With A:

$$A = time + \frac{1}{\mu_{max}} * log\,(exp\,(-\mu_{max} * time) + exp\,(-h_0) - exp\,(-\mu_{max} * time - h_0)) \quad (2)$$

With parameters (Table 3):

Literature review

For the literature review on MNP toxicity towards microalgae, the review papers of Podbielska and Szpyrka (2023) *'Microplastics – An emerging contaminants for algae. Critical review and perspectives'* and the review paper of Gorokhova et al. (2020) *'Micro- and Nanoplastic Exposure Effects Microalgae: A Meta-Analysis of Standard Growth Inhibition tests'* were used[92,93]. These were supplemented with papers on MNPs toxicity towards microalgae published after January 2023, found through Web of Science, and the ToMEX (The Toxicity of Microplastics Explorer 2.0) database[94] using the same exclusion criteria as those used by Podbielska and Szpyrka (2023). This brought the total of studies to 93. For each study, the test organism, polymer type, particle size and concentration range, included controls (such as an aging control and a natural particle control), and the studied end-points were compared. For ease of comparison, mass concentrations were converted to number concentrations, and vice versa, using mass conservation principles as discussed by Besseling et al., (2019). The complete list is in the supplementary materials (SI. 1).

Data availability

The datasets generated during and/or analysed during the current study are available from the corresponding author on reasonable request.

Received: 30 April 2025; Accepted: 27 August 2025
Published online: 26 September 2025

References

1. Falkowski, P. Ocean science: The power of plankton. *Nature* **483**, S17–S20 (2012).
2. Lindeman, R. L. The Trophic-Dynamic aspect of ecology. *Ecology* **23**, 399–417 (1942).
3. Falkowski, P. G. & Knoll, A. H. An Introduction to Primary Producers in the Sea: Who They Are, What They Do, and When They Evolved. in *Evolution of Primary Producers in the Sea* 1–6 Elsevier, (2007). https://doi.org/10.1016/B978-012370518-1/50002-3
4. Iversen, M. H. Carbon export in the ocean: A biologist's perspective. *Ann. Rev. Mar. Sci.* **15**, 357–381 (2023).
5. Ramanan, R., Kim, B. H., Cho, D. H., Oh, H. M. & Kim, H. S. Algae–bacteria interactions: evolution, ecology and emerging applications. *Biotechnol. Adv.* **34**, 14–29 (2016).
6. Lipsman, V., Shlakhter, O., Rocha, J. & Segev, E. Bacteria contribute exopolysaccharides to an algal-bacterial joint extracellular matrix. *NPJ Biofilms Microbiomes*. **10**, 36 (2024).
7. Sonnenschein, E. C., Syit, D. A., Grossart, H. P. & Ullrich, M. S. Chemotaxis of marinobacter adhaerens and its impact on attachment to the diatom Thalassiosira weissflogii. *Appl. Environ. Microbiol.* **78**, 6900–6907 (2012).
8. Flemming, H. C. et al. Biofilms: an emergent form of bacterial life. *Nat. Rev. Microbiol.* **14**, 563–575 (2016).
9. Xiao, R. & Zheng, Y. Overview of microalgal extracellular polymeric substances (EPS) and their applications. *Biotechnology Advances* **34**, 1225–1244 Preprint at https://doi.org/10.1016/j.biotechadv.2016.08.004 (2016).
10. Babiak, W. & Krzemińska, I. Extracellular polymeric substances (EPS) as microalgal bioproducts: A review of factors affecting EPS synthesis and application in flocculation processes. *Energies* **14**, Preprint at https://doi.org/10.3390/en14134007 (2021).
11. Neu, T. R. & Lawrence, J. R. Extracellular polymeric substances in microbial biofilms. in Microbial Glycobiology 733–758 (Elsevier, doi:https://doi.org/10.1016/B978-0-12-374546-0.00037-7. (2010).
12. Decho, A. W. & Gutierrez, T. Microbial extracellular polymeric substances (EPSs) in ocean systems. *Front Microbiol* **8**, 265214 (2017).
13. Wingender, J., Neu, R. & Thomas & Flemming; Hans-Curt. *Microbial extracellular polymeric substances*. Microbial Extracellular Polymeric Substances (Springer Berlin Heidelberg, doi:https://doi.org/10.1007/978-3-642-60147-7. (1999).
14. Zhang, Z. J., Chen, S. H., Wang, S. M. & Luo, H. Y. Characterization of extracellular polymeric substances from biofilm in the process of starting-up a partial nitrification process under salt stress. *Appl. Microbiol. Biotechnol.* **89**, 1563–1571 (2011).
15. Tang, J., Wu, Y., Esquivel-Elizondo, S., Sørensen, S. J. & Rittmann, B. E. How microbial aggregates protect against nanoparticle toxicity. *Trends Biotechnol.* **36**, 1171–1182 (2018).
16. Chen, B. et al. Role of extracellular polymeric substances from chlorella vulgaris in the removal of ammonium and orthophosphate under the stress of cadmium. *Bioresour Technol.* **190**, 299–306 (2015).
17. Mona, S. & Kaushik, A. Chromium and Cobalt sequestration using exopolysaccharides produced by freshwater Cyanobacterium Nostoc Linckia. *Ecol. Eng.* **82**, 121–125 (2015).
18. Su, Y. et al. Biodegradable and conventional microplastics posed similar toxicity to marine algae chlorella vulgaris. *Aquat. Toxicol.* **244**, 106097 (2022).
19. Khatiwada, J. R. et al. Interaction between polyethylene terephthalate (PET) microplastic and microalgae (Scenedesmus spp.): effect on the growth, chlorophyll content, and hetero-aggregation. *Environ. Adv.* **13**, 100399 (2023).
20. Li, R. et al. Effects of polystyrene nanoplastics on the physiological and biochemical characteristics of microalga scenedesmus quadricauda. *Environ. Pollut.* **319**, 120987 (2023).
21. Alam, M. A. et al. Characterization of the flocculating agent from the spontaneously flocculating microalga chlorella vulgaris JSC-7. *J. Biosci. Bioeng.* **118**, 29–33 (2014).
22. Manheim, D. & Nelson, Y. Settling and bioflocculation of two species of algae used in wastewater treatment and algae biomass production. *Environ. Prog Sustain. Energy*. **32**, 946–954 (2013).
23. González-Fernández, C. & Ballesteros, M. Microalgae autoflocculation: an alternative to high-energy consuming harvesting methods. *J. Appl. Phycol.* **25**, 991–999 (2013).
24. Shanks, A. L. & Trent, J. D. Marine snow: sinking rates and potential role in vertical flux. *Deep Sea Res. Part. Oceanogr. Res. Papers*. **27**, 137–143 (1980).
25. Kiørboe, T. & Hansen, J. L. Phytoplankton aggregate formation: observations of patterns and mechanisms of cell sticking and the significance of exopolymeric material. *J. Plankton Res.* **15**, 993–1018 (1993).
26. Frost, B. W. & EFFECTS OF SIZE AND CONCENTRATION OF FOOD PARTICLES ON THE FEEDING BEHAVIOR OF THE MARINE PLANKTONIC COPEPOD *CALANUS PACIFICUS* 1. *Limnol. Oceanogr.* **17**, 805–815 (1972).
27. Wilson, D. S. Food size selection among copepods. *Ecology* **54**, 909–914 (1973).
28. Rana, S. & Kumar, A. Toxicity of nanoparticles to algae-bacterial co-culture: knowns and unknowns. *Algal Res.* **62**, 102641 (2022).
29. You, X., Xu, N., Yang, X. & Sun, W. Pollutants affect algae-bacteria interactions: A critical review. *Environ. Pollut.* **276**, 116723 (2021).
30. Huang, S., Zhang, B., Liu, Y., Feng, X. & Shi, W. Revealing the influencing mechanisms of polystyrene microplastics (MPs) on the performance and stability of the algal-bacterial granular sludge. *Bioresour Technol.* **354**, 127202 (2022).
31. Hao, B. et al. Bacterial community are more susceptible to nanoplastics than algae community in aquatic ecosystems dominated by submerged macrophytes. *Water Res.* **232**, 119717 (2023).

32. Sioen, M. et al. Impact of weathered and Virgin polyethylene terephthalate (PET) micro- and nanoplastics on growth dynamics and the production of extracellular polymeric substances (EPS) of microalgae. *Science Total Environment* **953**, 176074 (2024).
33. OECD (2022). – processed by Our World in Data. OECD, Global Plastics Outlook - Plastics waste in 2019 by region, polymer and application. (2022).
34. Khoironi, A., Anggoro, S. & Sudarno, S. Evaluation of the interaction among microalgae spirulina sp, plastics polyethylene terephthalate and polypropylene in freshwater environment. *J. Ecol. Eng.* **20**, 161–173 (2019).
35. Piccardo, M. et al. PET microplastics toxicity on marine key species is influenced by pH, particle size and food variations. *Sci. Total Environ.* **715**, 136947 (2020).
36. Kaandorp, M. L. A., Lobelle, D., Kehl, C., Dijkstra, H. A. & van Sebille, E. Global mass of buoyant marine plastics dominated by large long-lived debris. *Nat. Geosci.* **16**, 689–694 (2023).
37. Besseling, E., Redondo-Hasselerharm, P., Foekema, E. M. & Koelmans, A. A. Quantifying ecological risks of aquatic micro- and nanoplastic. *Crit. Rev. Environ. Sci. Technol.* **49**, 32–80 (2019).
38. Hänninen, J. et al. Plastic debris composition and concentration in the Arctic ocean, the North sea and the Baltic sea. *Mar. Pollut Bull.* **165**, 112150 (2021).
39. Albertsson, A. C., Andersson, S. O. & Karlsson, S. The mechanism of biodegradation of polyethylene. *Polym. Degrad. Stab.* **18**, 73–87 (1987).
40. Seghers, J. et al. Approaches for the Preparation and evaluation of hydrophilic polyethylene and polyethylene terephthalate microplastic particles suited for toxicological effect studies. *Anal. Bioanal Chem.* https://doi.org/10.1007/s00216-024-05726-7 (2025).
41. Su, Y. et al. When microplastics Meet microalgae: unveiling the dynamic formation of aggregates and their impact on toxicity and environmental health. *Water Res.* **273**, 123008 (2025).
42. Ni, Z. et al. Toxic effects of pristine and aged polystyrene and their leachate on marine microalgae skeletonema costatum. *Sci. Total Environ.* **857**, 159614 (2023).
43. Gorokhova, E., Ek, K. & Reichelt, S. Algal growth at environmentally relevant concentrations of suspended solids: implications for microplastic hazard assessment. *Front Environ. Sci* **8**, 551075 (2020).
44. Alimi, O. S. et al. Weathering pathways and protocols for environmentally relevant microplastics and nanoplastics: what are we missing? *J. Hazard. Mater.* **423**, 126955 (2022).
45. Badmus, S. O., Amusa, H. K., Oyehan, T. A. & Saleh, T. A. Environmental risks and toxicity of surfactants: overview of analysis, assessment, and remediation techniques. *Environ. Sci. Pollut. Res.* **28**, 62085–62104 (2021).
46. Eisma, D. & Kalf, J. Distribution, organic content and particle size of suspended matter in the North sea. *Neth. J. Sea Res.* **21**, 265–285 (1987).
47. Food and Agriculture Organization of the United Nations. 2.3. Algal Production. FAO Corporate Document Repository. Fisheries and Aquaculture Department. (1996)
48. Finkel, Z. V. Does phytoplankton cell size matter?? The evolution of modern marine food webs. in Evolution of Primary Producers in the Sea 333–350 (Elsevier, doi:https://doi.org/10.1016/B978-012370518-1/50016-3. (2007).
49. Agusti, S., Duarte, C. M. & Kalff, J. Algal cell size and the maximum density and biomass of phytoplankton1. *Limnol. Oceanogr.* **32**, 983–986 (1987).
50. Luo, H. et al. Effects of accelerated aging on characteristics, leaching, and toxicity of commercial lead chromate pigmented microplastics. *Environmental Pollution* **257**, 113475 (2020).
51. Hermabessiere, L. et al. Occurrence and effects of plastic additives on marine environments and organisms: A review. *Chemosphere* **182**, 781–793 (2017).
52. *Hazard assessment report acetaldehyde Chemicals Evaluation and Research Institute (CERI)*, Japan. (2007). http://www.prtr.nite.go.jp/index-e.html
53. Patrick, R., Schleier, A. & Cairns, J. Jr. The relative sensitivity of diatoms, snails, and fish to Twenty common constituents of industrial wastes. *Progressive Fish-Culturist*. **30**, 137–140 (1968).
54. Brack, W. & Frank, H. *Chlorophyll a fluorescence: A tool for the investigation of toxic effects in the photosynthetic apparatus. ECOTOXICOLOGY Environ. SAFETY* **40,** 34-41 (1998).
55. Rummel, C. D., Schäfer, H., Jahnke, A., Arp, H. P. H. & Schmitt-Jansen, M. Effects of leachates from UV-weathered microplastic on the microalgae scenedesmus vacuolatus. *Anal. Bioanal Chem.* **414**, 1469–1479 (2022).
56. Almond, J., Sugumaar, P., Wenzel, M. N., Hill, G. & Wallis, C. Determination of the carbonyl index of polyethylene and polypropylene using specified area under band methodology with ATR-FTIR spectroscopy. *e-Polymers* **20**, 369–381 (2020).
57. Celik, M., Nakano, H., Uchida, K., Isobe, A. & Arakawa, H. Comparative evaluation of the carbonyl index of microplastics around the Japan Coast. *Mar. Pollut Bull.* **190**, 114818 (2023).
58. Gomes, S., Fernandes, R., Waldman, W. R. & A. N. & How to measure polymer degradation?? An analysis of authors' choices when calculating the carbonyl index. *Environ. Sci. Technol.* **58**, 7609–7616 (2024).
59. *Test No. 126: Determination of the Hydrophobicity Index of Nanomaterials Through an Affinity Measurement*. OECD, (2023). https://doi.org/10.1787/ae9c0fd1-en
60. Permana, R., Chakraborty, S. & Valsami-Jones, E. Nanoplastics in aquatic environments: the hidden impact of aging on fate and toxicity. *Environ. Chem. Ecotoxicol.* **7**, 429–444 (2025).
61. Hüffer, T., Praetorius, A., Wagner, S., Von Der Kammer, F. & Hofmann, T. Microplastic exposure assessment in aquatic environments: learning from similarities and differences to engineered nanoparticles. *Environ. Sci. Technol.* **51**, 2499–2507 (2017).
62. Wang, Q. et al. The toxicity of Virgin and UV-aged PVC microplastics on the growth of freshwater algae chlamydomonas reinhardtii. *Science Total Environment* **749**, 141603 (2020).
63. Shams, M., Alam, I. & Chowdhury, I. Aggregation and stability of nanoscale plastics in aquatic environment. *Water Res.* **171**, 115401 (2020).
64. Jahnke, A. et al. Reducing uncertainty and confronting ignorance about the possible impacts of weathering plastic in the marine environment. *Environ. Sci. Technol. Lett.* **4**, 85–90 (2017).
65. de Bono, J. & McDowell, G. Simulating multifaceted interactions between kaolinite platelets. *Powder Technol.* **413**, 118062 (2023).
66. Mitchel, J. K. & Soga, K. Fundamentals of Soil Behavior. *Soil Sci. Soc. Am. J.* vol. 40 (John Wiley & Sons, New Jersey, (2005).
67. Tadros, T. Electrostatic and Steric Stabilization of Colloidal Dispersions. in *Electrical Phenomena at Interfaces and Biointerfaces* 153–172 Wiley, (2012). https://doi.org/10.1002/9781118135440.ch10
68. Cheng, S., Jessica, Yoshikawa, K. & Cross, J. S. Influence of synthetic and natural microfibers on the growth, substance exchange, energy accumulation, and oxidative stress of field-collected microalgae compared with microplastic fragment. *Sci. Total Environ.* **908**, 167936 (2024).
69. Schwarzer, M. et al. Shape, size, and polymer dependent effects of microplastics on daphnia magna. *J. Hazard. Mater.* **426**, 128136 (2022).
70. Kim, D., Kim, H. & An, Y. J. Effects of synthetic and natural microfibers on daphnia magna–Are they dependent on microfiber type? *Aquat. Toxicol.* **240**, 105968 (2021).
71. Su, J. et al. Extracellular polymers substances towards the toxicity effect of microcystis flos-aquae under subjected to nanoplastic stress. *Environ. Pollut.* **372**, 125996 (2025).
72. Pančić, M. & Kiørboe, T. Phytoplankton defence mechanisms: traits and trade-offs. *Biol. Rev.* **93**, 1269–1303 (2018).

73. Gambardella, C. et al. Ecotoxicological effects of polystyrene microbeads in a battery of marine organisms belonging to different trophic levels. *Mar. Environ. Res.* **141**, 313–321 (2018).
74. Santschi, P. H. et al. Can the protein/carbohydrate (P/C) ratio of exopolymeric substances (EPS) be used as a proxy for their 'stickiness' and aggregation propensity? *Marine Chemistry* vol. 218 Preprint at https://doi.org/10.1016/j.marchem.2019.103734 (2020).
75. Shiu, R. F. et al. Nano- and microplastics trigger secretion of protein-rich extracellular polymeric substances from phytoplankton. *Science Total Environment* **748**,141469 (2020).
76. Xu, H. et al. Differential physiological response of marine and freshwater microalgae to polystyrene microplastics. *J. Hazard. Mater.* **448**, 130814 (2023).
77. Zhang, X. et al. Exploring cell aggregation as a defense strategy against perchlorate stress in chlamydomonas reinhardtii through multi-omics analysis. *Sci. Total Environ.* **905**, 167045 (2023).
78. Kiorboe, T. Formation and fate of marine snow: small-scale processes with large-scale implications. *Sci. Mar.* **65**, 57–71 (2001).
79. Azam, F. Microbial control of oceanic carbon flux: the plot thickens. *Sci. (1979)*. **280**, 694–696 (1998).
80. Bell, W. & Mitchell, R. Chemotactic and growth responses of marine bacteria to algal extracellular products. *Biol. Bull.* **143**, 265–277 (1972).
81. Kriest, I. & Evans, G. T. A vertically resolved model for phytoplankton aggregation. *Journal Earth Syst. Science* **109,** 453–469 (2000).
82. De Ruijter, V. N., Redondo-Hasselerharm, P. E., Gouin, T. & Koelmans, A. A. Quality criteria for microplastic effect studies in the context of risk assessment: A critical review. *Environ. Sci. Technol.* **54**, 11692–11705 (2020).
83. Guillard, R. R. L. & Hargraves, P. E. Stichochrysis immobilis is a diatom, not a chrysophyte. *Phycologia* **32**, 234–234 (1993).
84. Publishing Test No. 201: Alga, Growth Inhibition Test. OECD (2006). https://doi.org/10.1787/9789264069923-en
85. Chen, Z., Hay, J. N. & Jenkins, M. J. FTIR spectroscopic analysis of poly(ethylene terephthalate) on crystallization. *Eur. Polym. J.* **48**, 1586–1610 (2012).
86. Organisation for Economic Co-operation and Development (OECD). *Test No. 201: Freshwater Alga and Cyanobacteria, Growth Inhibition Test. Guidelines for the Testing of Chemicals, Sect. 2* (OECD Publishing, 2011).
87. Yang, S. & Li, X. fang Influences of extracellular polymeric substances (EPS) on the characteristics of activated sludge under non-steady-state conditions. *Process Biochemistry* **44**, 91–96 (2009).
88. Comte, S., Guibaud, G. & Baudu, M. Biosorption properties of extracellular polymeric substances (EPS) resulting from activated sludge according to their type: soluble or bound. *Process Biochem.* **41**, 815–823 (2006).
89. Heidelberg, B. *Microbial Extracellular Polymeric Substances* (Springer, 1999). https://doi.org/10.1007/978-3-642-60147-7
90. Kruger, N. J. The Bradford method for protein quantitation. 17–24 (2009). https://doi.org/10.1007/978-1-59745-198-7_4
91. Nielsen, S. S. Phenol-Sulfuric acid method for total carbohydrates. in 47–53 (2010). https://doi.org/10.1007/978-1-4419-1463-7_6
92. Podbielska, M. & Szpyrka, E. Microplastics – An emerging contaminants for algae. Critical review and perspectives. *Sci. Total Environ.* **885**, 163842 (2023).
93. Reichelt, S. & Gorokhova, E. Micro- and nanoplastic exposure effects in microalgae: A Meta-Analysis of standard growth Inhibition tests. *Front Environ. Sci* **8**, 560975 (2020).
94. Thornton Hampton, L. M. et al. A living tool for the continued exploration of microplastic toxicity. *Microplastics Nanoplastics.* **2**, 13 (2022).

Acknowledgements

This study was conducted with financial support from the Fonds voor Wetenschappelijk Onderzoek-Vlaanderen (FWO) project G053320N "Towards ecological risk assessment of nanoplastics: dynamic considerations". Maaike Vercauteren is funded by the Special Research Fund of Ghent University (Grant BOF21/PDO/081). Nanoplastics and nanoplastic characterization were supplied by the Joint Research Centre (JRC), with the support of John Seghers and Claudia Cella. The infrastructure used to produce the results presented in this work was funded by EMBRC Belgium - FWO international research infrastructure (ref. nr. I001621N). iFCM infrastructure and analysis, were provided by Peter Chaerle of BCCM/DCG and the Laboratory for Protistology & Aquatic Ecology (Ghent University). We thank Emmy Pequeur, Jolien Depecker and Nancy De Saeyer, for the lab support, and Jenevieve Hara from the University of Antwerp for assistance in the DLS characterization of the particles.

Author contributions

Marie Sioen: Conceptualization, Methodology, Software, Validation, Formal Analysis, Investigation, Writing – Original Draft, Visualization Maaike Vercauteren: Conceptualization, Methodology, Writing – Review & Editing Peter Chaerle: Conceptualization, Methodology, Software, Validation, Formal Analysis, Writing – Review & Editing Jana Asselman: Conceptualization, Methodology, Writing – Review & Editing, Funding acquisition, Supervision Colin R. Janssen: Conceptualization, Methodology, Writing – Review & Editing, Funding acquisition, Supervision Raewyn Town: Writing – Review & Editing, Funding acquisition, Supervision Ronny Blust: Writing – Review & Editing, Funding acquisition, Supervision.

Funding sources

This study was conducted with financial support from the Fonds voor Wetenschappelijk Onderzoek-Vlaanderen (FWO) project G053320N "Towards ecological risk assessment of nanoplastics: dynamic considerations". Maaike Vercauteren is funded by the Special Research Fund of Ghent University (Grant BOF21/PDO/081). The infrastructure used to produce the results presented in this work was funded by EMBRC Belgium - FWO international research infrastructure (ref. nr. I001621N).

Declarations

Competing interests

The authors declare no competing interests.

Additional information

Supplementary Information The online version contains supplementary material available at https://doi.org/10.1038/s41598-025-17863-9.

Correspondence and requests for materials should be addressed to M.S.

Reprints and permissions information is available at www.nature.com/reprints.

Publisher's note Springer Nature remains neutral with regard to jurisdictional claims in published maps and institutional affiliations.

Open Access This article is licensed under a Creative Commons Attribution-NonCommercial-NoDerivatives 4.0 International License, which permits any non-commercial use, sharing, distribution and reproduction in any medium or format, as long as you give appropriate credit to the original author(s) and the source, provide a link to the Creative Commons licence, and indicate if you modified the licensed material. You do not have permission under this licence to share adapted material derived from this article or parts of it. The images or other third party material in this article are included in the article's Creative Commons licence, unless indicated otherwise in a credit line to the material. If material is not included in the article's Creative Commons licence and your intended use is not permitted by statutory regulation or exceeds the permitted use, you will need to obtain permission directly from the copyright holder. To view a copy of this licence, visit http://creativecommons.org/licenses/by-nc-nd/4.0/.

© The Author(s) 2025